Journal of
Ceramic Science
and Technology

J. Ceram. Sci. Tech., **05** [04] 299-308 (2014)
DOI: 10.4416/JCST2014-00016
available online at: http://www.ceramic-science.com

Mullitization of Manganese-Doped Aluminosilicate Diphasic Gel

J. Roy*[1], S. Das[2], S. Maitra[2]

[1]Camellia Institute of Technology, Kolkata-700129, India
[2]Government College of Engineering & Ceramic Technology, Kolkata-700010, India
received April 24, 2014; received in revised form July 5, 2014; accepted August 19, 2014

Abstract

Diphasic mullite precursor gel was synthesized from inorganic salts of aluminum and silicon. The synthesized gel was characterized by means of chemical analyses, FTIR spectroscopic studies as well as measurement of surface area and bulk density. Manganese dioxide (MnO_2) as an additive was mixed with the dried gel in different ratios (w/w) by co-grinding followed by compaction. The compacted masses were sintered at different elevated temperatures. The mullitization process was studied by performing differential thermal analysis (DTA) at four different heating rates and the activation energy for mullitization was calculated in each case, using the Kissinger thermal analysis model. MnO_2 lowered the activation energy of the mullitization process. XRD and SEM techniques were used to study the microstructures and phase development in the sintered masses. It was observed that in presence of MnO_2, the microstructure of the mullite ceramics was significantly modified, resulting in an enhancement of the mechanical properties of mullite.

Keywords: Sol-gel method, ceramics, differential thermal analysis, scanning electron microscopy, x-ray diffraction

I. Introduction

Mullite is a non-stoichiometric aluminosilicate compound and it is the only thermodynamically stable phase in the SiO_2-Al_2O_3 binary system [1]. Its molecular formula is $Al_2[Al_{2+2x}Si_{2-2x}]O_{10-x}$, where x denotes the number of missing oxygen atoms per unit cell, varying between 0.17 and 0.59 [2]. Mullite is an important engineering material, as it has some remarkable properties which include good thermal and chemical stability, low creep rate, reasonable toughness and strength, infrared transparency, [3–6] etc. Owing to these important qualities, mullite is widely used in making refractory materials, computer chips, [7,8] etc. The most advanced applications of mullite are in electronic packaging, thin films, window material for the mid-infrared wavelength range, [9–12] etc.

The sol-gel process is one of the most advanced processes for the synthesis of mullite with high purity and better homogeneity. Based on the degree of homogeneity, the gel can be divided into two types: monophasic having a particle size at the atomic level and diphasic with a homogeneity scale in the nanometric range [13]. In the diphasic gel system, the heat of reaction of the different phases provides extra energy for the densification process [14].

To improve the overall mullitization process, transition metal cations as dopants can be incorporated in the mullite structure in different proportions [15]. Different experiments have been conducted on the sol-gel-derived transition-metal-oxide-doped mullite. da Silva [16] synthesized manganese-doped mullite by means of sol-gel and observed a manganese-inducedmullitization process at a lower temperature. Tkalcec *et al.* [17] reported that up to 9.60 wt% Cr_2O_3 could be incorporated in the mullite structure. Again chromium doping increased the unit-cell parameters of mullite with strongest expansion along the c-axis. Bagchi *et al.* [18] observed that mullite can be synthesized even at a temperature as low as 600 °C with the sol-gel process in the presence of nickel and cobalt ions at about 0.02 M concentration. Again the extent of mullite formation decreased with the increase in the transition metal ion concentration. Roy *et al.* [19] synthesized transition-metal-doped mullite ceramics with the sol-gel technique and observed that up to a certain concentration, mullite phase formation was accelerated in the presence of transition metal ions. In our earlier works [20–25], inorganic salts of aluminium and silicon were used to synthesize mullite by the sol-gel route and different 3d transition metal oxides were doped into it. We have observed that these transition metal cations help the mullitization process positively. So in this present work, by determining the activation energy of mullitization and analyzing the microstructure and mechanical properties of sintered products, we have studied the effect of manganese addition during mullitization of diphasic aluminosilicate gel.

II. Experimental

(1) Synthesis of manganese-doped mullite

For the synthesis of mullite precursor gel, the starting materials used were 5 % (w/v) aluminum nitrate nonahydrate [$Al(NO_3)_3{\cdot}9H_2O$, alumina (Al_2O_3) content 12.98 % w/w] extra pure (MERCK, India) and 5 % (w/v) liquid sodium silicate [sp. Gr. 1.6 and molar ratio

* Corresponding author: royj007@rediffmail.com

of Na_2O:SiO_2 =1:3, silica (SiO_2) content 29.75 % w/w] (LOBA CHEMIE, India). Silicic acid was prepared by passing liquid sodium silicate (7 % w/v) through an ion exchanger column packed with Dowex-50 cation exchanging resin at a flow rate of 200 ml/min. During ultrasonic dispersion of the silicic acid in aqueous phase, silica sol was obtained. Now $Al(NO_3)_3 \cdot 9H_2O$ solution and silica sol were mixed together in such a way that the weight ratio of alumina and silica in the mixture remained 73:27, which is slightly higher in alumina content than that in mullite (72:28) in order to avoid formation of glassy phase during mullitization. To this mixture, ammonia solution (1:1, v/v) was added slowly with constant stirring until the pH of the solution became ~ 9. Mixed sol was aged to obtain the gel. The gel was then filtered and washed thoroughly, before being dried at 80 °C.

The dried gel was calcined at 800 °C for 2 h. Then in a pot mill, one part of the calcined gel was mixed with reagent-grade manganese dioxide (MnO_2, MERCK, India, 99.97 % pure) additive in three different ratios (1, 2 and 3 % w/w) and thoroughly ground to ensure proper homogeneity in the mixture.

(2) Characterization

Chemical analysis (following the specifications in ISO 21587 – 2:2007), surface area (measured with a twin surface area analyzer, Quantachrome) and bulk density (measured with an Ultrapyc 1200e helium pycnometer) of the dried gel were measured and the results are given in Table 1. The dried gel was heat-treated at eight different temperatures from 200 to 1600 °C with an interval of 200 °C each and Fourier transformation infrared spectroscopy (FTIR) spectra of the dried gel and heat-treated samples were taken using a Perkin-Elmer apparatus (Model: Vertex-70).

Table 1: Physicochemical properties of the hydrogel

Composition	Properties
SiO_2 (wt%)	17.86
Al_2O_3 (wt%)	48.23
Ignition loss (%)	33.91
Bulk density (g/cm^3)	0.27
Sp. surface area (m^2/g)	70

Differential thermal analysis of both the calcined and doped gel were performed at four different heating rates 4, 6, 8 and 10 K/min from room temperature to 1400 °C using a differential thermal analyzer (Okay Libratherm instrument, Model: DTA-1500, Bysak, India). The activation energy of mullitization in the case of both undoped and doped samples was determined from DTA thermogram using the Kissinger equation [26].

The equation used is:

$$\ln\left(\frac{T_p^2}{\upsilon}\right) = \ln\left(\frac{E_a}{R}\right) - \ln\phi + \frac{E_a}{RT_p} \qquad (1)$$

where, T_p = temperature of the exothermic peak, ν = heating rate, E_a = activation energy, R = universal gas constant and φ = frequency factor.

According to Eq. (1), the plot of $\ln(T_p^2/\nu)$ versus $1/T_p$ will be a straight line and from the slope of the line, the value of activation energy can be evaluated.

The powder mixes were compacted at 100 MPa, and the compacted masses were fired in an electrically heated muffle furnace at three different final temperatures, 1400, 1500 and 1600 °C (heating rate was 10 K/min up to 1000 °C and then 2 K/min until the final temperature was reached), with 2 h soaking period in each case. The bulk density and apparent porosity of the sintered masses were measured in accordance with the procedures described in BS 1902, Part 1A, 1966 [27]. The flexural strength of the sintered samples were determined based on measurement of the bending strength with a span of 30 mm and a loading rate of 0.5 mm/min. Fracture toughness was determined with an indentation micro-crack method with a load of 5 kg [28]. The XRD pattern of the samples was taken with a Rigaku x-ray diffractometer with Cu target (Miniflex, Japan). The lattice parameters of both doped and undoped samples were calculated using the following equation,

$$\frac{h^2}{a^2} + \frac{k^2}{b^2} + \frac{l^2}{c^2} = \frac{1}{d^2} \qquad (2)$$

where, h, k, l are the Miller indices of the peaks in Cartesian coordinates, a, b, c are the lattice parameters and d is the spacing of the lattice planes.

The % d- error for the sample and JCPDS (5 – 0776) standard d-values for all planes are calculated using the following formula:

$$\text{Relative percentage error, i.-e., \% d error} = \frac{|d_{ex} - d|}{d} \times 100 \qquad (3)$$

where d_{ex} is the experimentally obtained d value and d is the standard d-value in the JCPDS file.

The average crystallite size was calculated using Debye-Scherrer formula [29],

$$D = 0.9\lambda/(\beta\cos\theta) \qquad (4)$$

where D is the diameter of the crystallites forming the film, λ is the wavelength of CuKα line, β is full width at half-maximum (FWHM) in radians, and θ is the Bragg angle.

$$\beta = \sqrt{(\beta_0)^2 - (b)^2} \qquad (5)$$

where β_o is the FWHM in radians for the sample and b is the FWHM in radians for the pure crystal.

Scanning electron microscopic investigation of the samples was performed with a FEI Quanta microscope (US).

III. Results and Discussion

The precursor gel had very low bulk density (0.27 g/cm^3) and high surface area (70 m^2/g), indicating high surface activity of the gel. The water content of the gel was almost 34 %. To prevent excessive shrinkage during sintering, the gel was calcined at 800 °C.

(1) FTIR spectral analysis of the undoped sample:

The FTIR spectra of the dried and heat-treated samples at different temperatures are shown in Figs. 1 and 2. In the spectra of the dried gel, bands that appeared at 3151 cm^{-1} and 1104 cm^{-1} were assigned to the Al-OH stretching and bending vibrations respectively. Appearance of a shoulder at 1104 cm^{-1} was related to the overlapping of Si-O-Si stretching vibration of SiO_4^{4-} tetrahedra with Al-OH bending vibration [30]. Si-O-Si bending vibration appeared at 477 cm^{-1}. Again stretching of Al-O-Al linkage was observed at 747 cm^{-1} [31]. But no characteristic peak corresponding to Al-O-Si linkage was observed in the FTIR spectra of the gel sample. It confirmed that the gel, aluminum hydroxide, $Al(OH)_3$ and silicon hydroxide, $Si(OH)_4$ allformed simultaneously. So the precursor gel was diphasic in nature.

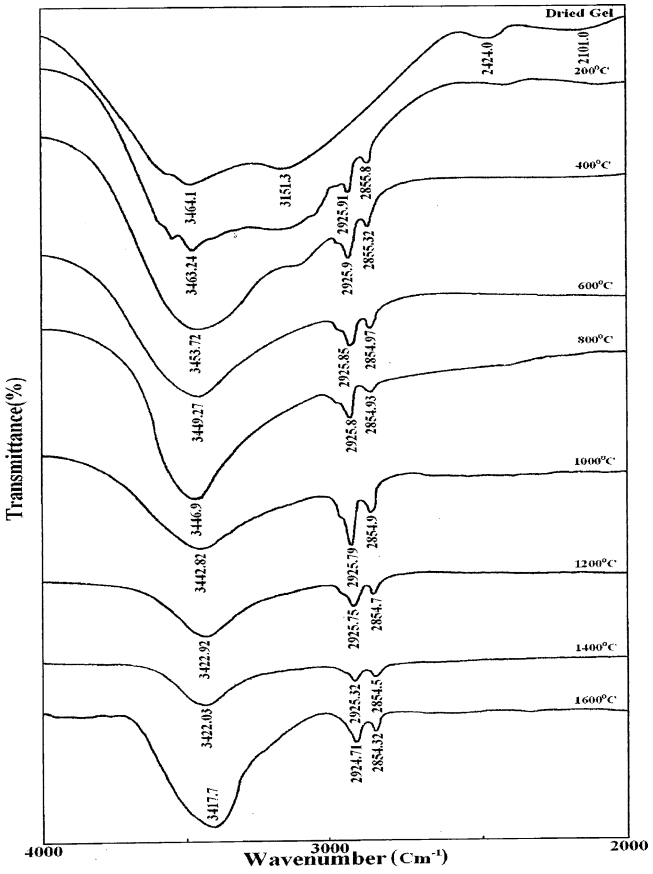

Fig 1: FTIR spectra of the aluminosilicate gel after heat treatment at different temperatures within 2000 – 4000 cm^{-1}.

Si-O-Al linkage first appeared in the spectra of the sample heated at 600 °C. The peak at 803 cm^{-1} was assigned to symmetric stretching vibration of Si-O-Si linkages. This peak was slightly shifted to 806 cm^{-1} in the spectra of the sample heated at 800 °C. This result confirmed the formation of Al-Si spinel in the gel structure. After heating at 1000 – 1200 °C, the major change in the spectra was observed in the shifting of peaks at 832 – 833 cm^{-1} from 806 cm^{-1}. This indicated the formation of more Si-O-Al linkages, resulting in crystallization of mullite phases. The peak observed at 843 cm^{-1} in the spectra of the sample heated at 1400 °C became wider, indicating the formation of more Si-O-Al linkages in the mullite crystals. Again peaks at 586 cm^{-1} owing to the stretching vibration of octahedrally coordinated Al became sharper, indicating the formation of Al_2O_3 in the structure. In the spectra of the sample heated at 1600 °C, the peak corresponding to Si-O-Si linkage became broader indicating complete crystallization of mullite [32].

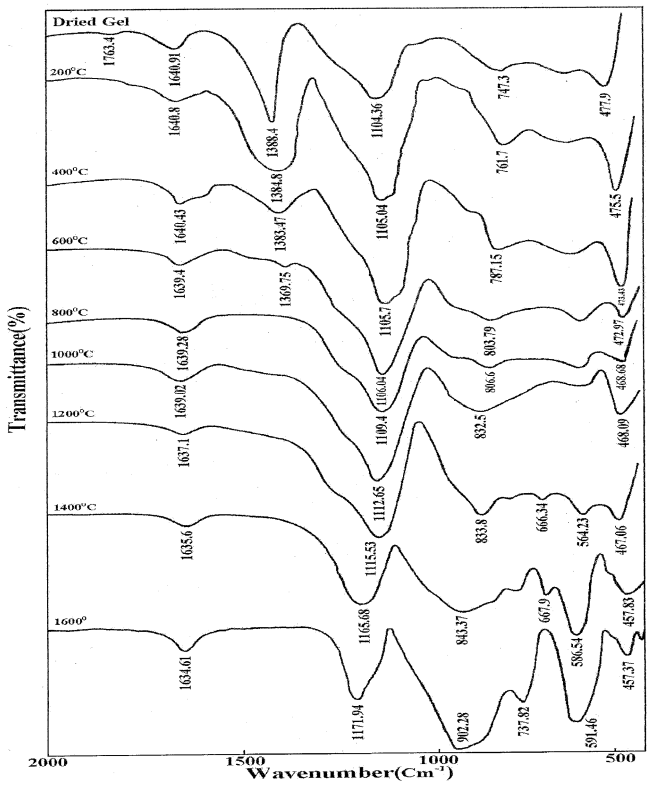

Fig 2: FTIR spectra of the aluminosilicate gel after heat treatment at different temperatures within 400 – 2000 cm^{-1}.

(2) Role of manganese ion as additive:

MnO_2 has a structure of linked MnO_6 octahedra that form "tunnels" capable of holding cations. Again MnO_2 has a low melting point (535 °C) [33, 34]. So it can generate mobile ions during sintering at high temperature, which are likely to substitute the Al^{3+} in AlO_6 octahedra generated from the crystallization of pseudo-boehmite gel. $Mn^{4+}(d^3)$ has a symmetric configuration as all the electrons exist in the lower energy t_{2g} level and do not interact with the electrons of the surrounding oxygen under the octahedral configuration. But it can distort the symmetry of SiO_4^{4-} tetrahedra by occupying the e_g level. The cationic size of Mn^{4+} under six coordination is 53pm, which is similar to that of Al^{3+} [33]. The cation generates defects in the alumina layer in the following way:

$$MnO_2 + Al_2O_3 \rightarrow Mn''_{Al} + O^{xx}_{O} + V'''_{Al} \qquad (6)$$

(3) Kinetics of mullitization

During FTIR spectral analysis, it was observed that Si-O-Al linkage started to form after heat treatment at 600 °C and continued up to 1400 °C. To know the onset temperature of mullitization and the effect of MnO_2 on it, differential thermal analysis of both undoped and doped samples

was performed and the results are shown in Fig. 3. It was observed that the mullitization process was exothermic in nature. The peak temperatures of mullitization were shifted towards higher temperature with increase heating rates. For undoped gel, primary mullitization was noticed in the temperature range of 975 – 990 °C, whereas in the case of the manganese-doped sample, mullitization was started at a lower temperature (946 – 966 °C). With increasing additive content, the exothermic peaks were shifted to a lower temperature but the change was very little (~1 – 2 K). Using Eq. (1), the plots of $\ln(T_p^2/\nu)$ versus $1/T_p \times 10^4$ are shown in Fig. 4, and the values of activation energy are given in Table 2. In the case of the undoped sample, the value of the activation energy of mullitization was equal to ~772 kJ/mol, which was lower than that available in the literature [26, 35, 36]. It can be related to the formation of diphasic gel in this present investigation. The activation energy of mullitization was much reduced with increasing additive content, which can be related to the defects generated owing to vacancies created in the aluminosilicate framework as a result of Mn^{3+}/Mn^{4+} incorporation. The reductions were almost 10, 15 and 17 % respectively in case of 1-%, 2-% and 3-%-doped samples. So with increasing manganese concentration, the rate of the mullitization process became faster.

Table 2: Values of activation energy

Sample	E in kJ/mol	Reduction of activation energy w.r.t undoped sample (%)
Calcined gel	772	-
1 % MnO_2	696	9.89
2 % MnO_2	658	14.80
3 % MnO_2	611	20.90

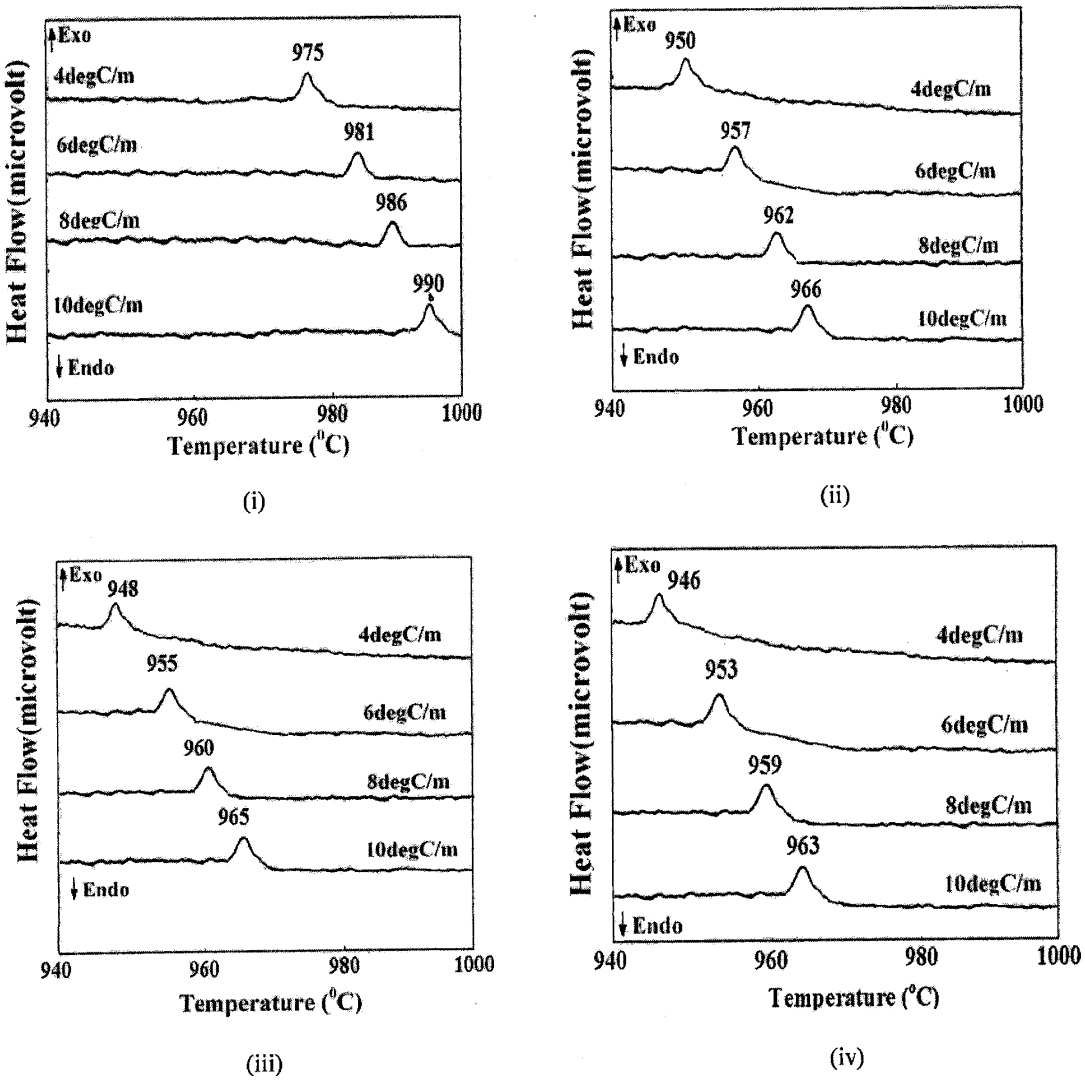

Fig. 3: DTA curves of (i) Undoped and (ii) 1 % (iii) 2 % (iv) 3 % MnO_2-doped gel sample.

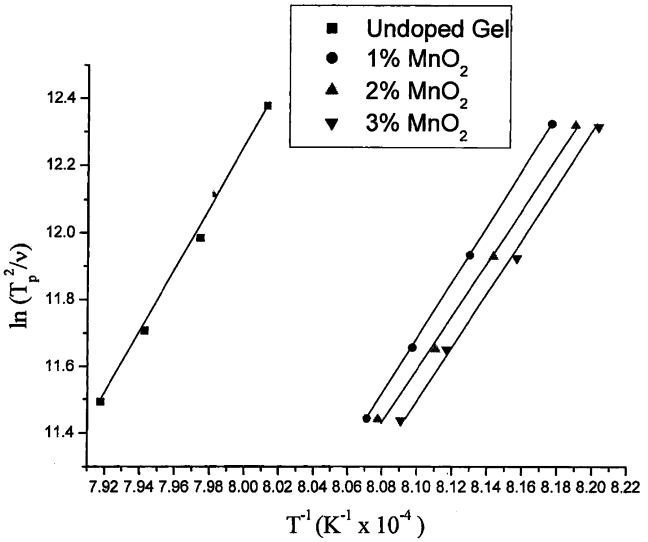

Fig. 4: Plot of ln (T_p^2/v) vs. T^{-1} x 10^{-4} of undoped and MnO_2-doped sample.

(4) Crystallographic information

The XRD of both undoped and doped samples are shown in Figs. 3A→3D. Both manganese silicate and manganese aluminate phases were observed in the x-ray diffractogram of the doped samples (Figs. 5→8). These phases promoted the formation of mullite by reducing the energy barrier for the reaction of alumina and silica. Again the relative proportion of mullite also increased with the increase in the both MnO_2 content and the sintering temperature.

The values of unit cell parameters of orthorhombic mullite are a =7.60Å, b =7.70Å, c =2.90Å [37–40]. Now the lattice parameters of both undoped and doped samples were calculated using Eq. (2) and the results are given in Table 3. In the case of the undoped sample, with the increase in sintering temperature, the structure became more perfect. For manganese-doped samples, the maximum deviation took place along the b axis. The change in cell volume was caused owing to the substitution of Al^{3+} by Mn^{4+} in the mullite structure. With the increase in sintering temperature and additive content, the cell volume of doped mullite decreased. This was due to the expulsion of Mn^{4+} from the mullite lattice and its accumulation at the grain boundary of mullite crystals.

From the XRD data, the % d-error, which is a measure of the shift in mullite crystal planes owing to structural deformation and/or incomplete formation, have also been calculated in presence of MnO_2 additive at different sintering temperatures using Eq. (3) and the results are given in Table 4. From the results, it can be presumed that with the increase of additive content and the sintering temperature, % d error decreased, implying that the crystal structure of mullite became more perfect.

The average crystallite size after calculation using Eq. (5) for the mullite sample with MnO_2 dopant is given in Table 5. With the increase in sintering temperature, the size of the mullite crystallites became shorter, suggesting the accumulation of a significant amount of MnO_2-bearing phases like manganese silicate at the grain boundary of the mullite samples.

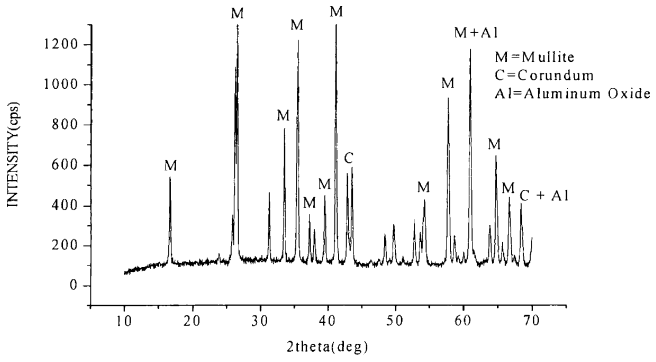

Uncalcined Gel

Fig. 5: XRD diagram of the gel (no additive) sintered at 1600 °C.

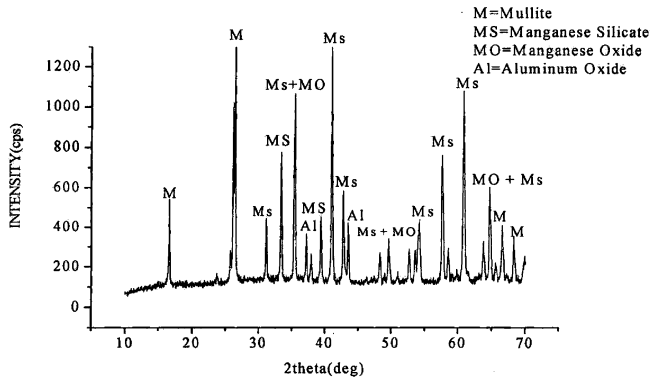

Fig. 6: XRD diagram of the sintered gel with 3 % MnO_2 at 1600 °C.

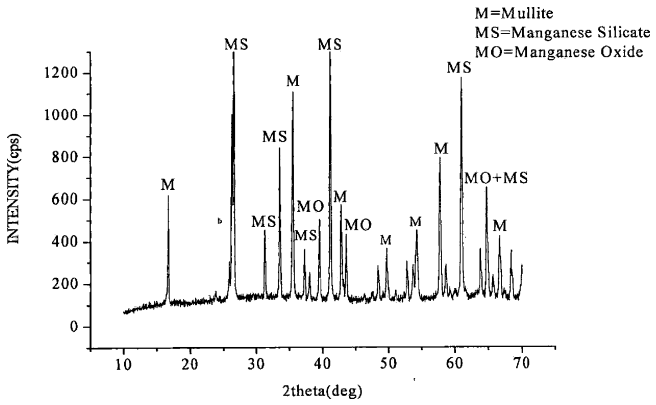

Fig. 7: XRD diagram of the sintered gel with 2 % MnO_2 at 1600 °C.

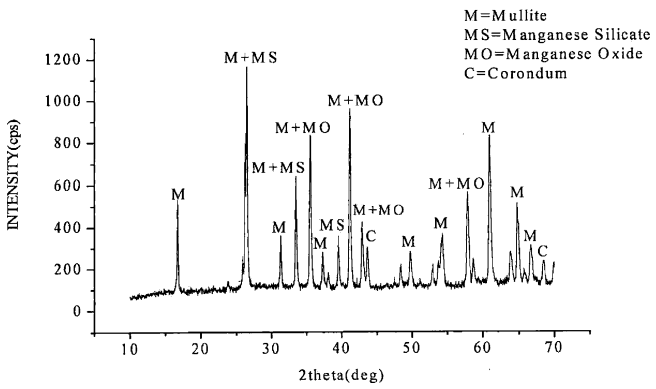

Fig. 8: XRD diagram of the sintered gel with 1 % MnO_2 at 1600 °C.

(5) Microstructural analysis

From the SEM micrographs of the sintered samples (Figs. 9 and 10), it is apparent that the incorporation of manganese ions in the sol-gel mullite induced tabular crystal growth parallel to the crystallographic c-axis. From the calculated values of lattice parameters it was observed that elongation of mullite crystals took place along the 'b' direction and lattice growth of the crystals around the 'c' direction. Elongated mullite crystals were observed to exist in a parallel fashion along the 'c' direction. With the increase in the manganese ion content in mullite, formation of more equiaxed but smaller sized crystallites was observed. Again the values of the average crystallite size were decreased with the increase in the sintering temperature, suggesting that the microstructure became more cohesive with the increase in the additive content.

Table 3: Values of lattice parameters of undoped and MnO_2-doped sample at different sintering temperature

Sample	Firing temperature (°C)	Theoretical cell parameters				Experimental cell parameters				Change in cell volume (%)
		a (Å)	b (Å)	c (Å)	abc $(Å)^3$	a (Å)	b (Å)	c (Å)	abc $(Å)^3$	
Undoped gel	1400	7.6	7.7	2.9	169.71	7.63	7.74	2.92	172.44	1.61
	1500					7.61	7.72	2.91	170.96	0.74
	1600					7.605	7.7	2.91	170.40	0.41
3 % MnO_2	1400					7.61	7.75	2.92	172.21	1.48
	1500					7.61	7.74	2.92	171.99	1.34
	1600					7.6	7.72	2.91	170.73	0.61
2 % MnO_2	1400					7.61	7.76	2.94	173.62	2.30
	1500					7.615	7.75	2.92	172.33	1.54
	1600					7.61	7.73	2.92	171.77	1.21
1 % MnO_2	1400					7.62	7.79	2.93	173.92	2.48
	1500					7.62	7.76	2.92	172.66	1.74
	1600					7.61	7.74	2.915	171.70	1.17

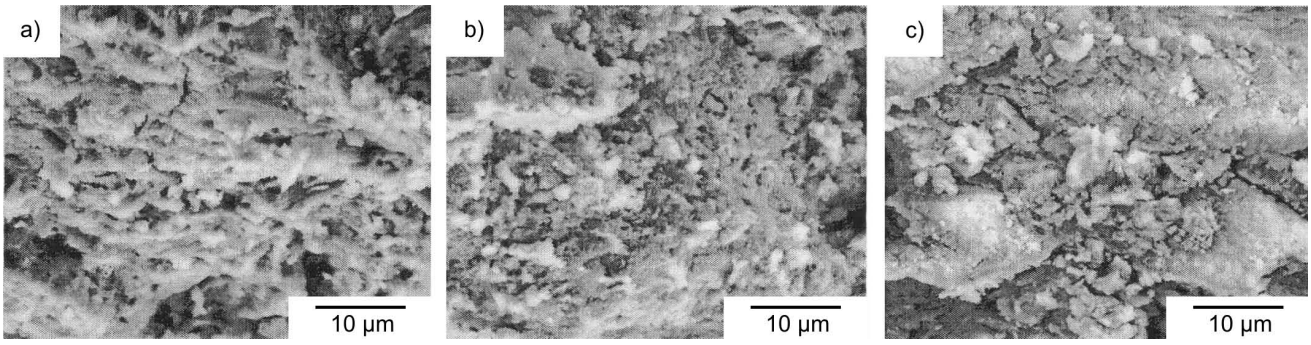

Fig. 9: Scanning electron micrograph of the sintered gel samples (no additive) (i): sintered at 1400 °C (ii) sintered at 1500 °C (iii) sintered at 1600 °C.

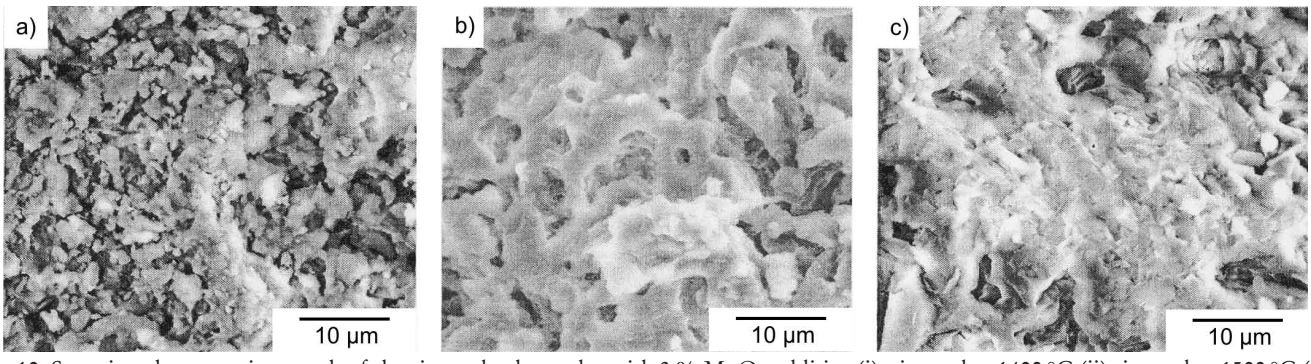

Fig. 10: Scanning electron micrograph of the sintered gel samples with 3 % MnO_2 additive (i): sintered at 1400 °C (ii) sintered at 1500 °C (iii) sintered at 1600 °C.

Table 4: % d-error for mullite phase in presence of MnO_2 additive at different sintering temperature.

Additive content (%) →	1	2	3
Sintering temperature (°C) ↓			
1400	2.29	2.12	1.90
1500	1.51	1.39	1.21
1600	1.29	1.11	0.98

Table 5: Average crystallite size (μm) of MnO_2 doped sample at different sintering temperature.

Additive content (%) →	1	2	3
Sintering temperature (°C) ↓			
1400	3.691	3.662	3.640
1500	2.794	2.576	2.257
1600	2.103	1.996	1.885

(6) Physico-mechanical properties

The variation in bulk density (Fig. 11) and apparent porosity (Fig. 12) of the samples with sintering temperature is shown in Table 6. From the results, it is clear that MnO_2 exhibited a positive effect on the densification of the mullite ceramics. After sintering at 1500 °C, there was no significant improvement in the apparent porosity values of the sintered samples whereas the bulk density of the samples increased linearly with the increase in sintering temperature from 1500 °C to 1600 °C. This can be attributed to the reduction of closed pores in the system. As discussed earlier, MnO_2 contains Mn^{4+} ions which could form defects in the Al_2O_3 sub-lattice as described by Eq.- (6). These induced defects resulted in enhanced densification during the sintering process. Owing to the low melting point of MnO_2 (~ 535 °C), during re-crystallization of mullite some manganese ions could come out of the crystal structure resulting in the formation some manganese silicate type liquid phases. This could be a reason for the enhanced densification of MnO_2-containing mullite samples at elevated temperatures with the significant reduction in closed porosity. The variation in flexural strength (Fig. 13) and fracture toughness (Fig. 14) of the samples with sintering temperature is shown in Table 6. MnO_2 also influenced the flexural strength and fracture toughness of the sintered mullite samples significantly. Both flexural strength and fracture toughness values were increased with increasing MnO_2 content. Owing to the low melting temperature, liquid phase formed by MnO_2 at high temperature in Al_2O_3-SiO_2 gel composition reduced the stress surrounding the pores in the sintered samples, displacing the gases inside the pores [41]. The reduction in porosity could be related to the improvement in mechanical strength. Again defects created by MnO_2 in the Al_2O_3-SiO_2 framework as shown in Eqs. (6) and (7) resulted in an improvement in the rate of densification in the sintered samples. Existence of a small amount of highly viscous silica-bearing phases on aluminosilicate glass phases would minimize the contribution of grain boundary sliding to fracture stress. Again formation of interlocked mullite crystalline phases in the presence of MnO_2 additive could be another reason for the improvement in mechanical strength. It has been observed that although properties like bulk density and flexural strength increase monotonically with the increase in the additive content, with apparent porosity there is no improvement above 2 % additive content. Therefore, the additive content was kept within 3 % in the present investigation.

Table 6: Variations in bulk density, apparent porosity, flexural strength and fracture toughness of MnO_2-doped sample at different sintering temperatures.

Property	Sintering temperature (°C)	Percentage composition (%)		
		1	2	3
Bulk density (increased)	1400	7	10	13
	1500	3	14	17
	1600	16	23	33
Apparent porosity (reduced)	1400	11	14	23
	1500	9	26	45
	1600	9	26	42
Flexural strength (increased)	1400	15	27	30
	1500	4	19	20
	1600	8	22	26
Fracture toughness (increased)	1400	2	10	11
	1500	2.5	5	12.5
	1600	4	7	10

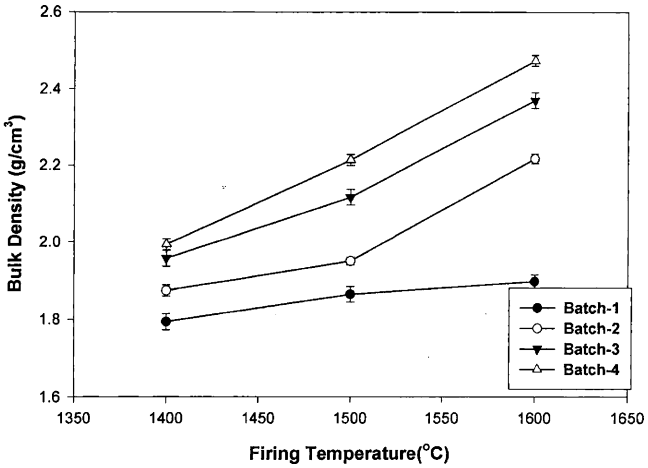

Fig. 11: Variation in bulk density of MnO_2-doped sintered aluminosilicate gel with firing temperature (°C).

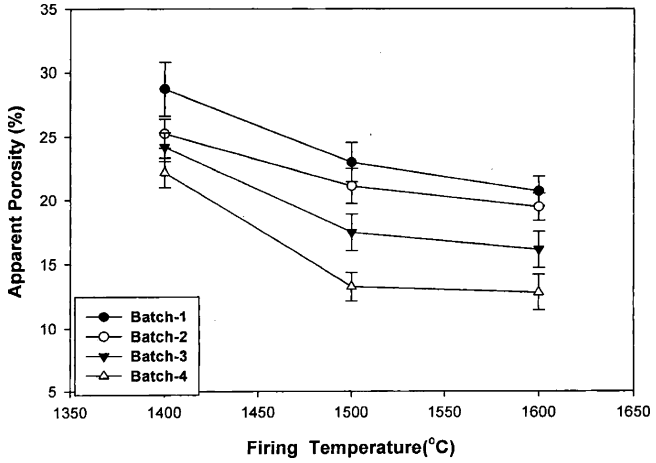

Fig. 12: Variation in apparent porosity (%) of MnO_2-doped sintered aluminosilicate gel with firing temperature (°C).

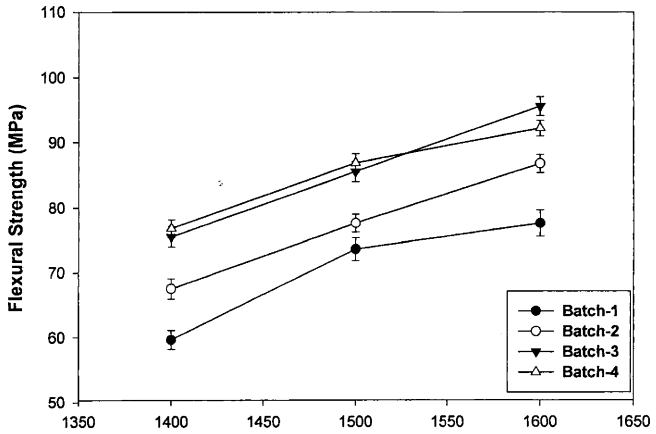

Fig. 13: Variation in flexural strength of MnO_2-doped sintered aluminosilicate gel with firing temperature (°C).

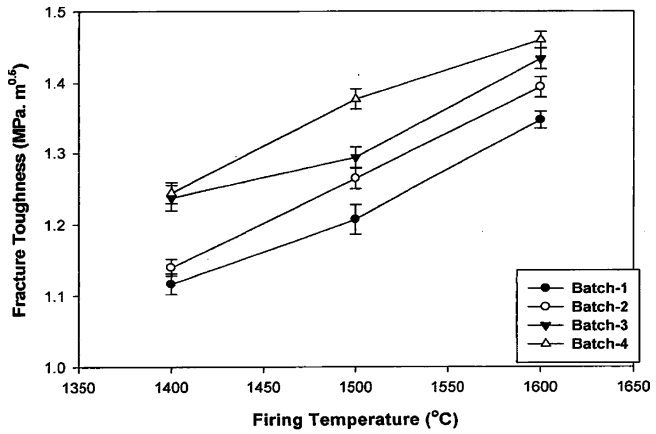

Fig. 14: Variation in fracture toughness of MnO_2-doped sintered aluminosilicate gel with firing temperature (°C).

IV. Conclusion

Mullite ceramics were synthesized from diphasic aluminosilicate gel formed by colloidal interaction of silicic acid and $Al(NO_3)_3$ solution. The gel powder possessed very low density and high surface area and consisted of separate non-linked units of alumina and silica gel. Different proportions of MnO_2 were used as sintering additive for the processing of mullite ceramics. Activation energy of mullitization was decreased with increasing metal ion concentration. The crystallite size of mullite was modified in the presence of MnO_2. The mechanical properties of the sintered mullite ceramics were also improved significantly owing to the enhanced microstructure and favourable phase compositions.

References

1 Bowen, N.L., Greig, J.W.: The system $Al_2O_3.2SiO_2$, *J. Am. Ceram. Soc.,* **7**, 238–254, (1924).

2 Cameron, W.E.: Mullite: a substituted alumina, *Am. Miner.,* **62**, 747–755, (1977).

3 Schneider, H., Eberhard, E.: Thermal expansion of mullite, *J. Am. Ceram. Soc.*, **73**, 2073–2076, (1990).

4 Hynes, A.P., Doremus, R.H.: High-temperature compressive creep of polycrystalline mullite, *J. Am. Ceram. Soc.,* **74**, 2469–2475, (1991).

5 Kollenberg, W., Schneider, H.: Microhardness of mullite at temperartures to 1000 °C, *J. Am. Ceram. Soc.,* **72**, 1739–1740, (1989).

6 Aksay, A., Dabbs, D.M., Sarikaya, M.: Mullite for structural, electronic and optical applications, *J. Am. Ceram. Soc.,* **74**, 2343–2358, (1991).

7 Skoog, A.J., Moore, R.E.: Refractory of the past for the future: mullite and its use as a bonding phase, *Am. Ceram. Soc. Bull.,* **67**, 1180–1185, (1988).

8 Kobayashi, F., Wanatabe, W., Yamamoto, N., Anzai, A., Takahashi, A., Daikoku, T., Fujita, T.: Hardware technology for hitachi M-880 processor group. In: proceedings of 41st electronic components & Technology Conf. Atlanta (GA), 1991.

9 Ramakrishnan, V., Goo, E., Roldan, J.M., Giess, E.A.: Microstructure of mullite ceramics used for substrate and packaging applications, *J. Mater. Sci.,* **27**, 6127–6130, (1992).

10 Kurihara, T., Horiuchi, M., Takeuchi, Y., Wakabayashi, S.: Mullite ceramic substrate for thin-film application. In: proceedings of 40th components and technology conf. IEEE, New York, 68–75, 1990.

11 Mazel, F., Gonon, M., Fantozzi, G.: Manufacture of mullite substrates from andalusite for the development of thin film solar cells, *J. Eur. Ceram. Soc.,* **22**, 453–461, (2002).

12 Shinohara, N., Dabs, D.M., Aksay, I.A.: Infrared transparent mullite through densification of monolithic gels at 1250 °C, Proc. SPIE—Int. Soc. Opt. Eng., **683**, 19–24, (1986).

13 Cividanes, L.S., Campos, T.M.B., Rodrigues, L.A., Brunelli, D.D., Thim, G.P.: Review of mullite synthesis routes by sol-gel method, *J. Sol-Gel Sci. Technol.,* **55**, 111–125, (2010).

14 Roy, R., Komarneni, S., Roy, D.M.: Better ceramics through chemistry. In: Brinker, C.J., Clark, D.E., Ulrich, D.R. (eds). Elsevier, North-Holland, New York, pp. 347–360, 1984.

15 Schneider, H: Transition metal distribution in mullite, *Ceram. Trans.*, **6**, 135–138, (1990).

16 da Silva, M.G.F.: Role of MnO on the mullitization behavior of Al_2O_3-SiO_2 gels, *J. Sol-Gel Sci. Technol.,* **13**, 987–990, (1998).

17 Tkalcec, E., Grzeta, B., Popovic, J., Ivankovic, H., Rakvin, B.: Structural studies of Cr-doped mullite derived from single-phase precursors, *J. Phys. Chem. Solids.* **67**, 828–835, (2006).

18 Bagchi, B., Das, S., Bhattacharya, A., Basu, R., Nandy, P.: Effect of nickel and cobalt ions on low temperature synthesis of mullite by sol-gel techniques, *J. Sol-Gel Sci. Technol.,* **55**, 135–141, (2010).

19 Roy, D., Bagchi, B., Bhattacharya, A., Das, S., Nandy, P.: A comparative study of densification of sol-gel derived nano-mullite due to the influence of iron, nickel and copper ions, *Int. J. Appl. Ceram. Technol.*, 2013 DOI: 10.1111/ijac.12114.

[20] Roy, J., Bandyopadhyay, N., Das, S., Maitra, S.: Effect of CoO on the formation of mullite ceramics from diphasic Al_2O_3-SiO_2 gel, *J. Engg. Sci. Technol. Rev.,* **3,** 136 – 141, (2010).

[21] Roy, J., Bandyopadhyay, N., Das, S., Maitra, S.: Effect of TiO_2 on the formation of mullite ceramics from diphasic Al_2O_3-SiO_2 gel, *Interceram,* **59**, 213 – 217, (2010).

[22] Roy, J., Bandyopadhyay, N., Das, S., Maitra, S.: Role of Cr_2O_3 on the formation of mullite ceramics from diphasic Al_2O_3-SiO_2 gel, *Ceramica (Braz.),* **56**, 273 – 278, (2010).

[23] Roy, J., Bandyopadhyay, N., Das, S., Maitra, S.: Role of V_2O_5 on the formation of chemical mullite from aluminosilicate precursor, *Ceram. Int.,* **36**, 1603 – 1608, (2010).

[24] Roy, J., Bandyopadhyay, N., Das, S., Maitra, S.: Effect of copper ions on mullite formation from aluminosilicate precursor, *Ceram-Silik,* **54**, 128 – 132, (2010).

[25] Roy, J., Bandyopadhyay, N., Das, S., Maitra, S.: Effect of synthetic Fe_2O_3 on the properties of mullite ceramics from diphasic Al_2O_3-SiO_2 gel, *J. Aus. Ceram. Soc.,* **46**, 15 – 22, (2010).

[26] Okada, K.: Activation energy of mullitization from various starting materials, *J. Eur. Ceram. Soc.,* **28**, 377 – 382, (2008).

[27] shop.bsigroup.com

[28] de la Lastra, B., Leblud, C., Leriche, A., Cambier, F., Anseau, M.R.: K_{IC} calculations for some mullite-zirconia composites prepared by reaction sintering, *J. Mat. Sci. Lett.*, **4,** 1099 – 1101, (1995).

[29] Skinner, K.G., Cook, W.H., Potter, R.A., Palmour, H.: Effect of TiO_2, Fe_2O_3 and alkali on mineralogical and physical properties of mullite type and mullite forming Al_2O_3-SiO_2 mixtures, *J. Am. Ceram. Soc.,* **36,** 349 – 356, (1953).

[30] Okada, K., Otsuka, N.: Characterization of the spinel phase from SiO_2-Al_2O_3 xerogels and the formation process of mullite, *J. Am. Ceram. Soc.,* **69**, 652 – 656, (1986).

[31] Orefice, B.L., Vasconcelos, W.L.: Sol-gel transition and structural evolution on multicomponent gels derived from the alumina-silica system, *J. Sol-Gel Sci. Tech.,* **9,** 239 – 249, (1977).

[32] Roy, J., Bandyopadhyay, N., Das, S., Maitra, S.: Studies on the formation of mullite from diphasic Al_2O_3-SiO_2 gel by fourier transform infrared spectroscopy, *Iran. J. Chem. Chem. Eng.,* **30**, 65 – 71, (2011).

[33] Greenwood, N.N., Earnshaw, A.: Chemistry of the elements. 2nd edition. Butterworth Heinemann, Oxford, 1998.

[34] Schneider, H., Okada, K., Pask, J.: Mullite and mullite ceramics. John Wiley and Sons Ltd., England, pp. 52 – 53, 1994.

[35] Okada, K., Kanedaa, J., Kameshimaa, Y., Yasumoria, A., Takei, T.: Crystallization kinetics of mullite from polymeric Al_2O_3-SiO_2 xerogels, *Mater. Lett.*, **57**, 3155 – 3159, (2003).

[36] Tan, H., Ding, Y., Zhang, H., Yang, J., Qiao, G.: Activation energy for mullitization of gel fibres obtained from aluminium isopropoxide, *Bull. Mater. Sci.,* **35**, 833 – 837, (2012).

[37] Pask, J.A.: Importance of starting materials on reactions and phase equilibria in the Al_2O_3-SiO_2 system, *J. Eur. Ceram. Soc.,* **16**, 101 – 108, (1996).

[38] Li, D.X., Thomson, W.J.: Mullite formation from nonstoichiometric diphasic precursors, *J. Am. Ceram. Soc.,* **74**, 2382 – 2387, (1991).

[39] Ossaka, J.: Tetragonal mullite-like phase from co-precipitated gels, *Nature*, **191**, 1000 – 1001, (1961).

[40] Li, D.X., Thomson, W.J.: Tetragonal to orthorhombic transformation during mullite formation, *J. Mater. Res.,* **6**, 819 – 824, (1991).

[41] Gupta, S., Dubikova, M., French, D.: Effect of CO_2 gasification on the transformation of coke minerals at high temperatures, *Energy Fuels,* **21,** 1052 – 1061, (2007).